Results of an Experimental Study for 3D Ultrasound CT

N.V. Ruiter, G.F. Schwarzenberg, M. Zapf, A. Menshikov, and H. Gemmeke
Forschungszentrum Karlsruhe, Institute of Data Processing and Electronics, Germany, Email: ruiter@ipe.fzk.de

Introduction

The possible benefits of Ultrasound Computer Tomography (USCT) for breast cancer diagnosis have been known for a long time. The first publications in this field date back to the late 70s [1]. Building such a device for clinical practice in 2D or even 3D never succeeded; mostly due to the huge data rate and time consuming image reconstruction. Since then several scientists have been working on 2D ultrasound tomography. The proposed 2D setups only partly use the capability to focus ultrasound everywhere in the imaged object as diverging cylindrical wavefronts integrate over different amounts of volume at different time steps and thus decrease the resolution in the third dimension. High resolution in each dimension requires a 3D aperture of unfocussed transducers.

The presented 3D USCT arranges nearly 2000 unfocussed ultrasound transducers around the imaged object and records its interaction of ultrasonic waves from many different angles. The main advantage of such a system is simultaneous recording of reflection, absorption and speed of sound images, high image quality, and fast data acquisition. The aim of this first experimental setup for 3D USCT (Fig. 1) was to analyze the feasibility of such a system built with today's technology and draw conclusions for future steps.

Methodology

3D Setup for USCT

The 3D setup consists of a cylindrical vessel with 18 cm diameter and 15 cm height filled with water. The cylindrical walls are covered with ultrasound transducers, connected to a dedicated data acquisition hardware. The image reconstruction is carried out on separate PCs.

At the surface of the cylinder 384 emitting and 1536 receiving transducers are embedded. The cylinder can be rotated, adding up to 2304 virtual emitter and 9216 virtual receiver positions. Sequentially, each emitter sends an approx. spherical wave front, during this emission all receivers record simultaneously the pressure signals (A-scans) caused by ultrasound transmission, reflection, and scattering.

The ultrasound transducers are grouped into 48 transducer array systems (TAS). The transducers are dedicated to either emit or receive to increase the signal-to-noise ratio (SNR) of each channel. Each TAS incorporates eight emitters and 32 receivers with integrated amplifiers. An embedded signal generator codes the excitation of the emitters digitally. A single transducer has an active area of $(1.4\ \mathrm{mm})^2$ and is a piezo-composite with a sub-diced structure of three by three elements.

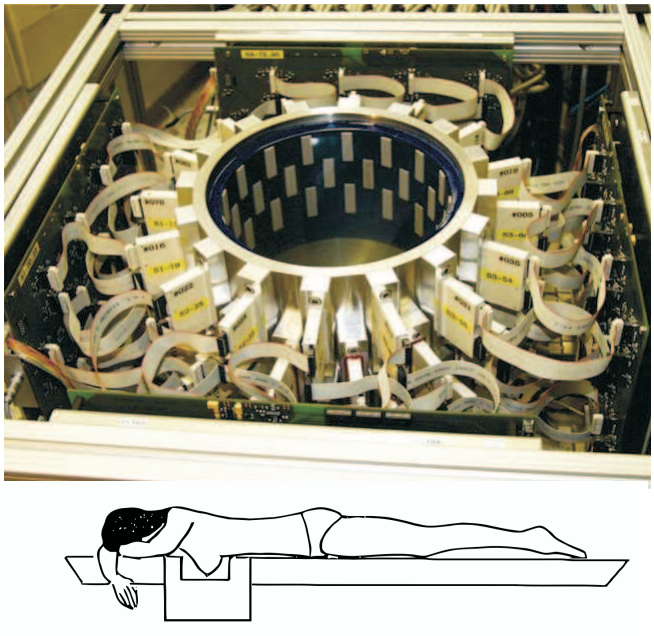

Figure 1: Top: Cylindrical aperture for a first experimental 3D setup for Ultrasound Computer Tomography. Bottom: Schematic drawing of imaging procedure.

The resulting opening angle is $\pm 15°$ at -6 dB for 2.4 MHz center frequency and was chosen as compromise between beam width and ultrasound pressure. The -6 dB bandwidth of the transducers is 1.4 MHz (52%). An average maximal sound pressure of 5 kPa at 10 mm distance was measured for 15 V maximal excitation. The A/D conversion samples with 10 MHz and 12 Bit.

The A-scans are recorded for 0.3 ms and additional 0.3 ms are allowed for the ultrasound signals to fade away, resulting in approx. 20 GBytes of raw data and a minimal data acquisition (DAQ) time of 6 s. This DAQ time cannot be reached at the moment due to the insufficient on-board memory and read-out speed, resulting in 8 h of DAQ for the whole volume. Therefore with this prototype only static phantoms may be studied.

3D Image Reconstruction Methods

The here applied reconstruction algorithm for reflectivity images is a synthetic aperture focusing technique (SAFT):

$$r(\mathbf{p}) = \sum_{j,k} T(A_{j,k}(t(\mathbf{p}))), \qquad (1)$$

where r denotes the reconstructed qualitative image of local impedance differences, $\mathbf{p}$ the reconstructed point, $A_{j,k}$ is the A-scan acquired at emitting position $\mathbf{e}_j$ and receiving position $\mathbf{r}_k$. T denotes different preprocessing of the A-scan. The equation assumes small attenuation, weak point scatterers, and spherical emittance. The time

t is related to the point $\mathbf{p}$ by

$$t(\mathbf{p}) = \frac{\|\mathbf{p} - \mathbf{e}_j\| + \|\mathbf{r}_k - \mathbf{p}\|}{\hat{c}(\mathbf{p}, \mathbf{e}_j, \mathbf{r}_k)}. \quad (2)$$

For the simplest reconstruction the average speed of sound may be assumed to be constant $\hat{c}(\mathbf{p}, \mathbf{e}_j, \mathbf{r}_k) = \hat{c}$, e.g. the speed of sound of water at the temperature measured during image acquisition.

Speed of sound and qualitative absorption images are reconstructed by evaluating the time and amplitude of the transmitted pulse and using the Feldkamp-Davis-Kress (FDK) [2] algorithm for inverse Radon projection in a cone beam geometry.

Signal Preprocessing

The possibility to assess the unfocussed data is crucial for this system, as coherent imaging, i.e. unprocessed addition of the delayed A-scans at the current point, is degrading the images due to phase aberrations in the data larger than $\lambda/2$, with λ the wavelength at the center frequency. The phase aberrations are caused by deviations of the transducers, and deviations of the average speed of sound $\hat{c}$ due to temperature drift and different materials in the object. Due to the longer and more different paths of the ultrasound in the USCT, these deviations are more pronounced than in conventional systems. Three approaches to cope with the phase aberration were compared.

Envelope

Envelope transformation of the A-scans before summation, i.e.

$$T(A(t)) = |H(A(t))| \quad (3)$$

is the absolute of the Hilbert transform H. It solves partly the problem with phase aberration as negative interference cannot occur, also the implementation is simple and the computation is fast. The drawbacks are reduction of the resolution and non-zero-mean addition of noise.

Adapted Matched Filtering

An often applied filter to increase SNR in ultrasound data is matched filtering [3]. A matched filter optimizes the SNR in case of white noise by correlating the signal with the known pulse form; here the applied excitation of the emitters. After the matched filter, an envelop transformation and detection of the local maxima for additional denoising is carried out. To account for the phase aberration the resulting signal is convoluted by a pulse with a lower bandwidth f_{new}. The optimal pulse $p_{\text{opt},f_{\text{new}}}(t)$ for reflectivity imaging as introduced by Norton and Linzer [4] is applied,

$$p_{\text{opt},f_{\text{new}}}(t) = 2 \cdot \text{sinc}(2f_{\text{new}} \cdot t) - \text{sinc}(f_{\text{new}} \cdot t)^2. \quad (4)$$

In sum the preprocessing is then

$$T(A(t)) = \big(\text{locMax}(|H(A(t) \star p(t))|)\big) * p_{\text{opt},f_{\text{new}}}(t), \quad (5)$$

where locMax denotes the local maximum, $\star$ the cross-correlation operator, $p(t)$ the applied excitation function for the emitters, and $*$ the convolution operator.

Table 1: Measured SNR in dB for Different Averaging and Bandpass

Averaging	1	4	8	16	32
Original data	44.0	52.0	55.0	58.3	61.0
Bandpass	56.5	62.6	65.7	68.3	71.6

The advantages of this method are simple and fast computation and denoising of the data. The empirically determined amount of phase aberration can be directly modeled and due to the envelope transformation sudden phase shifts are adjusted. Disadvantages are that changes in the pulse shape may change the position of the maxima and introduce blurring.

Adapted Matched Filtering using Chirps

The previous method is additionally adapted by applying frequency coded chirps as emitter excitation. Chirps allow long pulse duration to increase the SNR, and maintain the bandwidth as short pulses can be recovered by matched filtering.

Results

Data Acquisition

Noise and Averaging

The noise level of the system was measured in terms of

$$\text{SNR} = 20 \cdot \log_{10} \frac{A_{\max}}{\sqrt{\frac{1}{N}\sum_n A(n \cdot \triangle t)^2}},$$

with $A_{\max} = 2^{11}$ is the maximal amplitude, N the number of samples, and $\triangle t = 0.1$ μs the time step in the discretized data. The dependency on the averaging (1, 4, 8, 16, 32) and bandpass filtering (Hanning filter with pass band from 0.9 to 3.9 MHz) was analyzed. The measurements of the overall noise levels are displayed in table 1.

The maximal SNR for 12 Bit data and noise only in the least significant bit is 66.2 dB. With averaging an increase of SNR of 3 dB ($= 20\log_{10}(\sqrt{2})$) for each power of two is expected in case of white noise, which is approximately given in the results. The bandpass filter results in an average SNR increase of 11 dB. In summary, for a full utilization of the quantization, averaging of 8 or higher, and filtering by a bandpass has to be applied.

Sensitivity of Sensors

The sensitivity $\phi_{\mathbf{e}_j}$ and $\phi_{\mathbf{r}_k}$ of the individual transducers was estimated based on an empty measurement, i.e. only water in the USCT, and may be applied as multiplicative constant for each A-scan.The sensitivity of the transducers showed a relatively high standard deviation of $\sigma = 0.3$ for the emitters and $\sigma = 0.4$ for the receivers, partly due to a number of failing transducers; the standard deviation without these outliers is $\sigma = 0.2$ for the emitters and for the receivers.

Shift and Distribution of Temperature

The temperature changes were monitored with a calibrated GMH 3750 digital thermometer (Greisinger elec-

tronic GmbH, Germany), which is embedded in the lining of the inner cylinder and has direct contact to the water. Three sources of temperature change could be identified: a self heating effect, a layering effect, and changes of the air temperature. The internal gradient between the center of USCT and the cylinder walls is stable after approx. 1 h and amounts to approx. 1°C. The layering effect causes a temperature gradient at different depths. The difference between the top and bottom of the cylinder is 0.2°C.

A maximal deviation of 0.12°C can be tolerated for coherent SAFT reconstruction [6]. Currently, the temperature is monitored at a single position and this temperature is used to calculate the current speed of sound of the water.

Image Resolution

In USCT the 3D point spread function (PSF) is ideally only dependent on the center frequency, bandwidth, and 3D positioning of the transducers. The focussing during postprocessing assures ideal focus everywhere. The locality of the PSF is decreased due to the sparse aperture; the side lobes can be reduced by increasing bandwidth, the grating lobes by increasing number of transducers. In [5] we could show the PSF for the current cylindrical aperture to be rice corn shaped with an ideal width of 0.2 mm and height of 0.9 mm in the center of the USCT. To overcome the phase aberration, in the adapted matched filter approaches the optimal pulses were demodulated to 1.6 MHz before reconstruction. The expected full width half maximum (FWHM) of this setup is therefore approx. 0.4 mm.

Ten nylon threads with an diameter of 0.2 mm were immersed in water at the center of the USCT. The applied excitation was a pulse with center frequency of 2.4 MHz and bandwidth of 2 MHz. The averaging was set to 32. The water temperature ranged from 28 to 29°C. The images in Fig. 2 show reconstructions with different methods to cope with the phase aberration. The image size is $(2.3\ \mathrm{cm})^2$ and the pixel resolution is 0.023 mm. For all reconstructions only a subset of A-scans was used: Emitters and receivers with vertical position between [-0.15, 0.15] cm, where 0 cm corresponds to vertical position of reconstructed slice, angle between emitter and receiver $<90°$. The contrast in terms of signal difference to noise ratio (SDNR) and the resolution in terms of FWHM were evaluated for the resulting images.

Coherent imaging (not depicted) resulted not in closed points, due to negative interference with phase aberrations larger than $\lambda/2$. The SDNR for the envelope preprocessing was 0.5 and the mean FWHM 2.10 mm, due to the high background level. The adapted matched filter resulted in SDNR of 7.6 and a mean FWHM of 0.98 mm and the chirp data in in SDNR of 11.0 and a mean FWHM of 0.62 mm, giving good contrast and approaching the expected resolution.

The resolution of the transmission volumes is limited by the sparse aperture to 6 mm in vertical and 36 mm in the horizontal plane. Due to the limited opening angle many of the transmission pulses have low SNR, causing the reconstructed volumes to be very noisy. Experiments with a clinical breast phantom and gelatine phantoms showed that the speed of sound volumes are too noisy to distinguish small lesions. However the local average speed of sound is precise enough to enable phase aberration correction for reflectivity imaging when using envelope or adapted matched filter approaches [6].

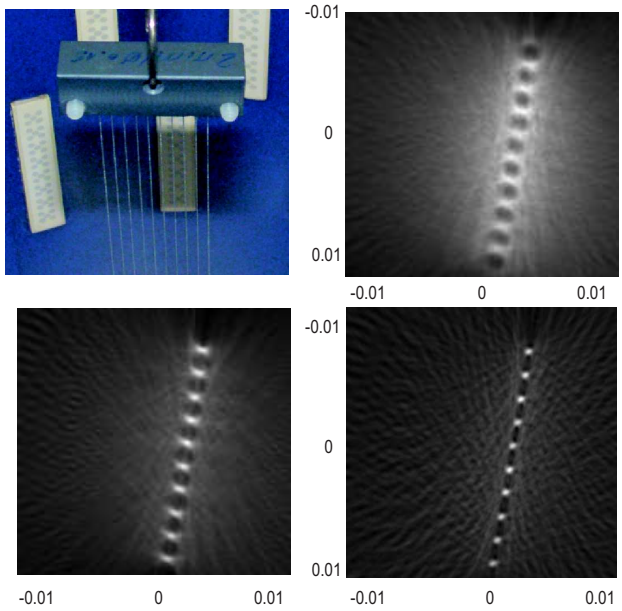

Figure 2: Top left: Experimental setup of ten nylon threads with diameter of 0.2 mm and distance of 2 mm. Top right to bottom left: Reconstructed images of coherent imaging with envelope, adapted matched filter, and adapted matched filter with Chirp excitation. Scaling in mm.

Discussion and Conclusion

Our first experimental 3D USCT showed that this technique is feasible with today's technology, if a sparse aperture or long DAQ times can be accepted. Therefore, the next question is, if the resulting volumes with current image quality have clinical relevance and can improve early breast cancer diagnosis. To answer this question, we are building a second generation 3D USCT setup with the main aim to image volunteers and carry out a preclinical study.

Based on simulations of the 3D PSF, image contrast and illumination, a more optimal aperture in form of a semi-ellipsoid is proposed for the next generation 3D USCT [7], see Fig. 3 and 4. The optimized semi-ellipsoidal aperture will be equipped with 640 emitters and 1440 receivers. The aperture can be rotated and lifted.

The new system offers fast DAQ with comparable or larger number of virtual transducers. The new DAQ hardware provides 480 parallel channels. The current problem of data read out will be solved by 40 GB of on-board memory. With a multiplex factor of 3 a minimum DAQ time of 6 s can be reached. Additional time will be needed to move the aperture and for averaging of the signals; we expect an overall DAQ time below 3 min.

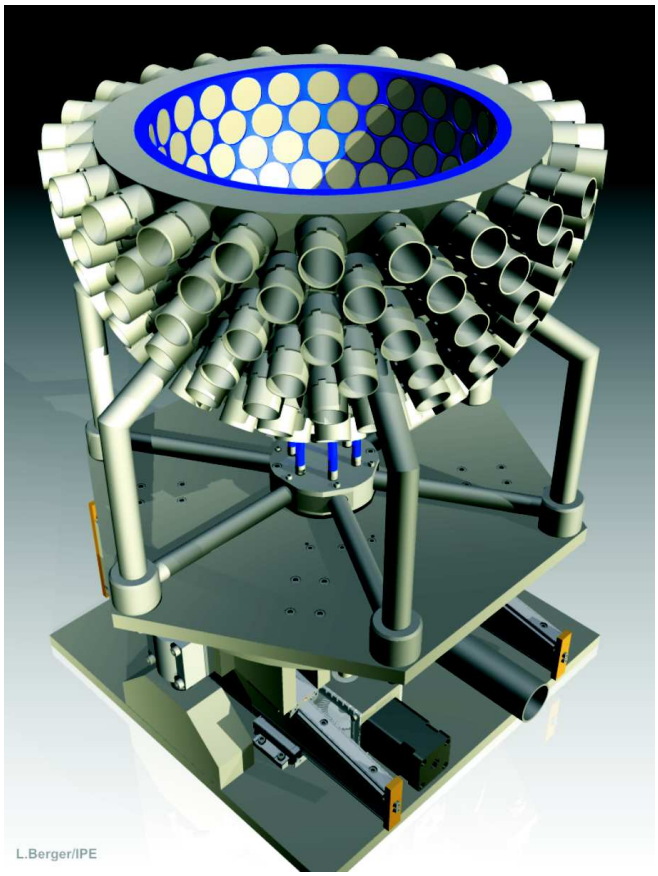

Figure 3: The image shows a technical drawing of the new semi-ellipsoidal aperture, new cylindrical TAS and the movement devices.

This will enable imaging of living tissue.

The basic concept of the current TAS will be maintained. A new grouping (four emitters and nine receivers) on a circular surface allows better approximation of the now semi-ellipsoidal aperture. The current variability of the sensitivity will be reduced by more restrictive quality control during the TAS fabrication. The active area of the individual transducers will be decreased for an opening angle of $\pm 25°$ to improve the SNR of the speed of sound maps and restrict the spatial variability of the 3D PSF in reflectivity imaging.

The resolution and image quality of our current system is limited by phase aberration error and sparse aperture. In simulations the mean resolution, measured by the size and deformation of the 3D PSF, is increased by 62% by the new aperture. The illumination of the breast volume is approx. three times higher than for the current cylindrical aperture. The artifacts are decreased by 23%. We expect a reduction of the remaining phase aberration error by the temperature monitoring and shorter DAQ time, a larger opening angle of the transducers for better speed of sound images and calibration of the TAS positions.

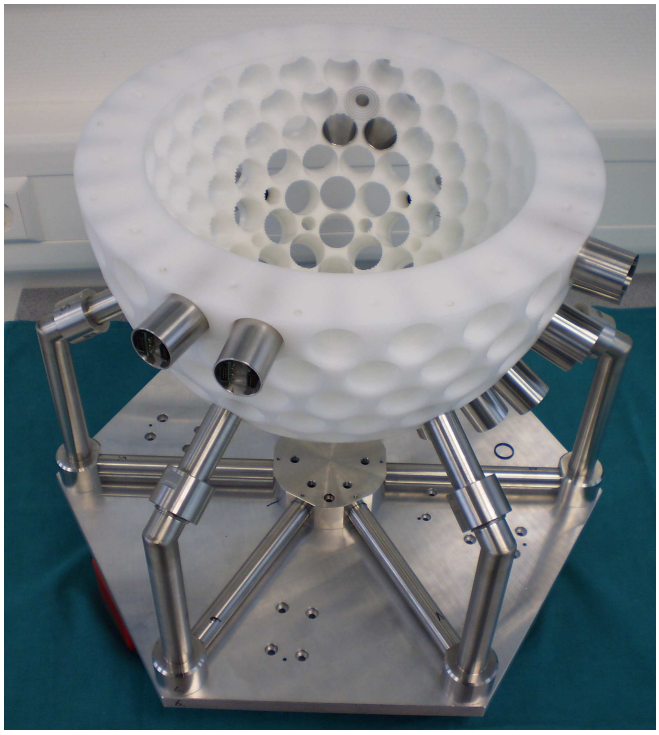

Figure 4: Current status of new sensor aperture.

References

[1] H. Schomberg: *An improved approach to reconstructive ultrasound tomography*, J. Phys. D: Appl. Phys., 11, pp. L181-L185, 1978.

[2] L. A. Feldkamp, L. C. Davis and J. W. Kress, *Practical Cone-Beam Algorithm*, J. Opt. Soc. Am., 1 (A):612–619, 1984.

[3] D.G. Manolakis, V.K. Ingle, S.M. Kogon: *Statistical and adaptive signal processing: spectral estimation, signal modeling, adaptive filtering and array processing*, McGraw-Hill publishers, Boston, 2000.

[4] S.J. Norton, M. Linzer: *Ultrasonic reflectivity tomography: Reconstruction with circular transducer arrays*, Ultrasonic Imaging 1, pp. 154-184, 1979.

[5] G.F. Schwarzenberg, R. Stotzka, M. Zapf, H. Gemmeke, N.V. Ruiter: *Resolution assessment of a 3D Ultrasound Computer Tomograph using Ellipsoidal Backprojection*, Proc. IEEE UFFC, pp. 1979-1982, 2006.

[6] N.V. Ruiter, R. Schnell, M. Zapf, H. Gemmeke: *Phase aberration correction for 3D Ultrasound Computer Tomography Images*, pp.1808-1811, Proc. IEEE UFFC, 2007.

[7] G.F. Schwarzenberg, M. Zapf, N.V Ruiter: *Aperture Optimization for 3D Ultrasound Computer Tomography*, Proc. IEEE UFFC, pp. 1820-1824, 2007.